Regional climate consequences of large-scale cool roof and photovoltaic array deployment

2011 Environ. Res. Lett. 6 034001

(http://iopscience.iop.org/1748-9326/6/3/034001)

Environ. Res. Lett. **6** (2011) 034001 (9pp) doi:10.1088/1748-9326/6/3/034001

Regional climate consequences of large-scale cool roof and photovoltaic array deployment

Dev Millstein and Surabi Menon

Lawrence Berkeley National Laboratory, Berkeley, CA, USA

E-mail: dmillstein@lbl.gov

Received 22 March 2011
Accepted for publication 13 June 2011
Published 1 July 2011
Online at stacks.iop.org/ERL/6/034001

Abstract

Modifications to the surface albedo through the deployment of cool roofs and pavements (reflective materials) and photovoltaic arrays (low reflection) have the potential to change radiative forcing, surface temperatures, and regional weather patterns. In this work we investigate the regional climate and radiative effects of modifying surface albedo to mimic massive deployment of cool surfaces (roofs and pavements) and, separately, photovoltaic arrays across the United States. We use a fully coupled regional climate model, the Weather Research and Forecasting (WRF) model, to investigate feedbacks between surface albedo changes, surface temperature, precipitation and average cloud cover. With the adoption of cool roofs and pavements, domain-wide annual average outgoing radiation increased by 0.16 ± 0.03 W m^{-2} (mean $\pm$ 95% C.I.) and afternoon summertime temperature in urban locations was reduced by 0.11–0.53 °C, although some urban areas showed no statistically significant temperature changes. In response to increased urban albedo, some rural locations showed summer afternoon temperature increases of up to +0.27 °C and these regions were correlated with less cloud cover and lower precipitation. The emissions offset obtained by this increase in outgoing radiation is calculated to be 3.3 ± 0.5 Gt CO_2 (mean $\pm$ 95% C.I.). The hypothetical solar arrays were designed to be able to produce one terawatt of peak energy and were located in the Mojave Desert of California. To simulate the arrays, the desert surface albedo was darkened, causing local afternoon temperature increases of up to +0.4 °C. Due to the solar arrays, local and regional wind patterns within a 300 km radius were affected. Statistically significant but lower magnitude changes to temperature and radiation could be seen across the domain due to the introduction of the solar arrays. The addition of photovoltaic arrays caused no significant change to summertime outgoing radiation when averaged over the full domain, as interannual variation across the continent obscured more consistent local forcing.

Keywords: photovoltaics, cool roofs, CO_2 offsets, radiative forcing, urban environment

S Online supplementary data available from stacks.iop.org/ERL/6/034001/mmedia

1. Introduction

Cool roofs and pavements reduce heating loads by reflecting more solar energy than surfaces they replace. For example, Akbari and Konopacki (2005) indicate solar reflectance for standard roofs is close to 0.2, while solar reflectance of a cool roof may be 0.5 or 0.6. Significant building-wide energy savings due to installations of cool roofs has been found in modeling studies (Pomerantz *et al* 1999) and measured in field studies (Akbari *et al* 1997, Akbari 2003). To reduce energy use, policies mandating the use of cool roofing materials have been adopted by many US states and are under study in the EU (Akbari and Levinson 2008, Synnefa *et al* 2009). Looking

beyond building-level energy savings, cool surfaces have been studied as a method for reducing urban temperatures and ozone concentrations (Taha 2008b, 2008c), and potentially, for reducing radiative forcing on a global scale (Akbari *et al* 2009, Menon *et al* 2010, Oleson *et al* 2010).

Many studies have examined the sensitivity of urban heat islands to urban albedo brightening. For example, Campra *et al* (2008) observed temperature reductions as construction of high albedo greenhouses spread through the Almeria region in southeastern Spain. Other studies have investigated urban albedo brightening using mesoscale meteorological models. Taha (2008c) found ∼1–2 °C decreases in peak urban temperatures at six locations across California. Synnefa *et al* (2008) and Lynn *et al* (2009) found similar results in Athens, Greece and New York City, respectively. Zhou and Shepherd (2009) found roughly ∼2 °C decreases in peak urban temperatures at Atlanta, however, temperature reductions were not a linear function of the magnitude of the simulated albedo increase. In one study at Houston (Taha 2008a), increased urban albedo did not consistently lead to temperature reductions and temperature changes ranged from −3.5 to +1.5 °C. It was suggested that feedback from decreased mixing might increase temperatures in certain situations.

The simulations described in Taha (2008c, 2008a), Synnefa *et al* (2008), Lynn *et al* (2009), and Zhou and Shepherd (2009), were run over a short-time span (1–4 days) with fine resolution ($\leqslant$ 4 km). The fine resolution allows for detailed treatment of urban physics, inclusion of urban morphology, and detailed representation of additional heat island mitigation strategies, such as increasing vegetation. These features can help tailor heat island mitigation policies for specific regions. Additionally, the fine resolution can capture more of the variation of response to albedo changes compared to coarsely resolved simulations. However, these simulations may hide feedbacks that develop only over longer time periods and larger domains.

There have been fewer studies that have addressed the issue of urban albedo change from a global perspective. Akbari *et al* (2009) use a simple radiative transfer calculation and find adoption of cool urban surfaces (increasing roof and pavement albedo by 0.25 and 0.15, respectively) could lower total global radiative forcing by 0.044, or 0.15 W m^{-2} averaged over global land area. Menon *et al* (2010) modeled global adoption of high albedo roofs and pavements by increasing the reflectance of urban areas by 0.1 finding an average increase of 0.5 W m^{-2} in total outgoing radiation over global land area. In their work, Menon *et al* (2010) employed a detailed land-surface model, but did not interactively couple the land model to a general circulation model, thus, atmospheric feedback resulting from urban albedo change was not investigated. Oleson *et al* (2010) use a coupled urban/atmospheric model to simulate global adoption of cool roofs. Oleson *et al* (2010) found the annual average urban heat island was reduced from 1.2 to 0.8 °C when roof albedo was increased to 0.9, however due to the coarse resolution of their simulations, analysis of atmospheric feedbacks resulting from urban albedo changes was not available.

The intent of this work is to resolve city-level albedo effects, investigate feedbacks found on a regional scale and a seasonal time frame, and aggregate results to a continental scale. To achieve this goal we use a regional atmospheric model with a fully coupled representation of the land-surface and atmospheric system and a domain with a spatial resolution of 25 km that covers the continental United States.

A second and parallel goal of this work is to investigate the effects of desert albedo changes due to the installation of large photovoltaic (PV) power plants. Nemet (2009) used a set of simple equations to compare the reduction of radiative forcing from PV substitution for fossil fuels to the increase in radiative forcing from increased albedo of the PV cells. Nemet (2009) found emission reductions due to PV substitution reduced radiative forcing by an amount 30 times greater than the radiative forcing increase from PV albedo changes, however, under certain conditions the albedo effect could substantially reduce the radiative forcing benefits of PV substitution.

Here we use a fully coupled atmospheric model to simulate the effects of darkening the albedo in the southern California desert corresponding to installation of a terawatt of solar arrays. A terawatt of peak capacity PV is a target value to reduce a gigaton of CO_2 emissions per year (Kantner *et al* 2009). We investigate local and regional atmospheric effects as well as changes to radiative forcing due to the PV adoption.

The methodology used in this study is described in section 2 and includes description of the modeling setup and evaluation of the output against observations. Results and discussion follow in section 3 and radiative forcing and equivalent CO_2 offsets due to albedo changes are presented.

2. Methods

2.1. Model details

The Weather Research and Forecasting (WRF) model version 3.2.1 was used in this study (Skamarock *et al* 2008). The modeling domain spans the continental United States, and ranges from 22 N, 121 W to 49 N, 64 W (see figure 1). The domain is divided horizontally into 200 × 128 grid cells, each square with an area of 625 km^2. The vertical dimension is divided into a telescoped 30 layers, with the top of the lowest layer reaching ∼55 m above ground or sea level and the highest layer reaching up to ∼16 km above sea level. Within WRF, the Noah land-surface model was used to simulate soil moisture, soil temperature, canopy moisture and fractional snow cover. The Noah land-surface model is based on previous work described in Chen and Dudhia (2001) and (Ek *et al* 2003). The planetary boundary layer was simulated using the Yonsei University scheme and the surface physics were modeled using the MM5 similarity surface layer scheme. Microphysics was modeled using the Lin *et al* (1983) scheme, which includes both mixed and ice phase processes and six different categories for hydrometers. Longwave radiation was modeled using the new Rapid Radiative Transfer Model (RRTMG) that includes the Monte Carlo Independent Column Approximation (McICA) for cloud overlap. The Goddard scheme for shortwave radiation was used and includes ozone effects based on climatological profiles and cloud effects. Cumulus physics was modeled with the Grell 3d ensemble cumulus scheme. Further details on the model methods listed

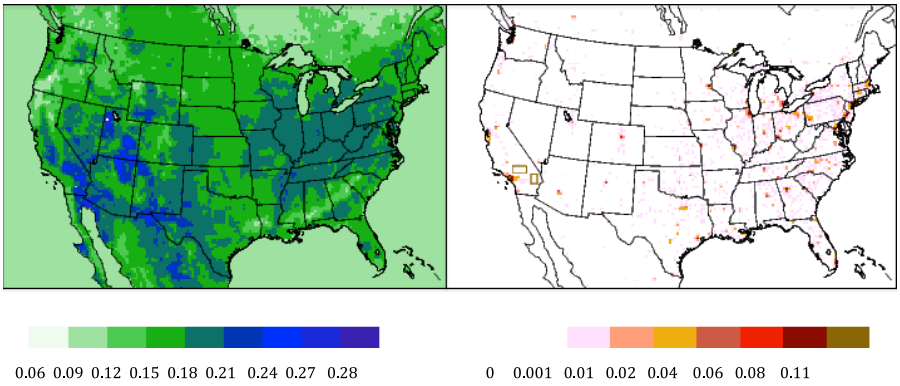

Figure 1. Left: surface albedo for CTRL in July. Right: Δ albedo (COOL–CTRL) and the outline of solar arrays modeled in SOL are shown. Please note non-linear color scheme in right panel.

above can be found in the recent WRF3.2 technical note (Skamarock *et al* 2008).

Initial and boundary conditions for all model runs were based on the three hourly, 32 km, North American Regional Reanalysis (NARR) data (Mesinger *et al* 2006). The monthly background surface albedo inputs were based on measurements made by the advanced very high resolution radiometer (AVHRR) on a polar orbiting satellite (Csiszar and Gutman 1999). Land use was derived from the USGS 24-category data set. The percentage of land area in the domain classified as urban was 0.7%. Alternatively, a MODIS land-use data set available with the WRF3.2.1 release, but was not used in this work as it was not compatible with all the land-surface modules available in WRF. The MODIS dataset classifies 1.1% of the domain as urban area. Advection of moisture, scalars, and turbulent kinetic energy (tke) was modeled using the positive definite advection options. Sea surface temperature was updated daily based on the AVHRR product from NOAA (Reynolds *et al* 2007). Gravity wave drag was included in the model formulation. Vertical velocity damping was employed over the top 1 km of the domain to help with model stability.

2.2. Scenarios

Three scenarios were compared in this work. The control (CTRL) and cool surfaces (COOL) cases were run continuously from January 1st, 1998 through December 30th, 2009. A third case investigating the installation of solar generating systems in the desert (SOL) was run only over 12 summer periods (1998–2009). The decision to include only summers in SOL was made due to limited computing resources and is justified by the low sensitivity of air temperature and other diagnostics to albedo changes during the winter months relative to summer months (a more detailed discussion of seasonality follows in section 3). SOL was initialized in March of each year with the relevant information extracted from CTRL. SOL outputs from months March through May of each year were discarded as spin up and outputs from June through August were analyzed.

COOL differs from CTRL only in that the surface albedo has been scaled to simulate adoption of cool roofs and cool pavements across all urban areas in the domain. Following Akbari *et al* (2009) we assume a roof and pavement urban area fraction of 25 and 35%, respectively, and +0.25 and +0.15 as the average increase in albedo with adoption of cool roof and cool pavement technology, respectively. The change to urban albedo from full adoption of cool roof and pavement technology is estimated to be $0.25 \times 0.25 + 0.15 \times 0.35 = +0.115$. The change to gridded albedo was calculated as $0.115 \times$ (fraction of urban area per grid cell). Few grid cells contained 100% urban area, thus, albedo changes ranged from 0.0 to +0.115 and are shown in figure 1.

SOL differs from CTRL only in that the surface albedo over a portion of the Mojave desert has been lowered to simulate the installation of large solar photovoltaic arrays. In total 30 grid cells were modified covering 18 750 km^2 of land area. The locations of the simulated solar farms (two locations, see figure 1: 34.7265 N, −117.91 W to 35.4051 N, −116.68 W, and 33.9918 N, −115.484 W to 34.741 N, −115.113 W) were chosen to be near proposed solar developments, for example the Abengoa Mojave Solar project and the Genesis Solar Energy project (CEC 2010a, 2010b). For reference, if there are 110 W of capacity for every m^2 of panels (11% efficiency), and roughly one half of the land area of each modified cell is covered in panels, then 30 modified grid cell could produce roughly 1 TW at peak capacity. 1 GW of capacity is often used as a reference size for a conventional power plant.

The albedo of the solar panels was set at 5% following (Nemet 2009), and the efficiency of solar panels was assumed to be 11%, similar to current efficiencies published by First Solar for the Cadmium Telluride FS-380 panel. The modified grid cells were set to have an albedo of 16%, assuming 5% of incoming solar radiation was reflected and 11% was removed from the location as electricity. A simplification was included in the calculation of the grid cell albedo as the panels were assumed to cover the entire surface area of each modified grid cell. Actual solar farms cover only a portion (one third to one half) of the total surface area. It is unclear if the albedo of the unused land would retain its original value or be altered by the installation and maintenance of the solar farm. Another simplification is that the modified albedo is not a function of season. The true dependence of the albedo of a solar farm on season is made complicated by the various panel technologies

and solar tracking technologies. Given these assumptions, SOL likely represents a lower bound to the effective albedo of a photovoltaic solar farm as efficiencies in all panel technologies have been increasing over time, efficiencies in silicon based panels are higher (14–19%), and concentrating photovoltaic systems are higher still (>20%).

2.3. Model evaluation

To evaluate model results, surface temperature anomalies, precipitation, outgoing longwave radiation, and surface incident shortwave radiation from CTRL were compared to satellite and ground based measurement data for a sample year 2005, with analysis extended for temperature comparisons across the full 12-year scenario.

Monthly average temperature is compared to 18 surface locations selected across the domain. Surface locations represent both urban and rural areas and low and middle elevations. To compare temperature anomalies, the difference between monthly average ground measurements and monthly climatological averages at each observation location were compared to corresponding differences of model outputs to a gridded climatological record derived from NARR (Mesinger *et al* 2006). Climatological data for ground stations was obtained from the US Climate Normals product (NOAA 2004) and the measurements spanning the model time period were obtained from NASA GISSTEMP (GISS 2010). Supplemental table 1 (available at stacks.iop.org/ERL/6/034001/mmedia) shows correlation between modeled and observed anomalies with the model accounting for ∼55% of the variance at most sites across all months.

The National Weather Service provides gridded observed precipitation for 2005 based primarily on radar and gauge measurements (NWS 2010). Supplemental figure 1 (available at stacks.iop.org/ERL/6/034001/mmedia) compares accumulated precipitation over 2005 between the model and observations. Across Washington, Oregon and California both annual totals and the spatial distribution of precipitation matched well. Across the rest of the country the spatial patterns of precipitation matched well but a tendency toward positive bias in model precipitation was found. In general the positive bias was more pronounced during summer months.

Satellite measurements of outgoing longwave radiation based on the AIRS instrument on Aqua were produced with the Giovanni online data system, developed and maintained by the NASA GES DISC (Acker and Leptoukh 2007). Both satellite measurements and model data were averaged afternoon values, satellite observations occurred between noon—3 pm local time and modeled data was averaged at 1 PM PST (2100 UTC). Supplemental figure 2 (available at stacks.iop.org/ERL/6/034001/mmedia) shows monthly outgoing longwave averages from the model and satellite observations. Spatial patterns matched well across seasons. During the summer the model showed lower (5–10%) outgoing long wave radiation in the southwest and higher (∼10%) outgoing radiation over much of the eastern half of the US compared to satellite measurements. During the winter, the model also shows 5–20% differences compared with satellite measurements.

Table 1. Albedo and temperature changes (°C) at 1 pm PST in urban areas.

			Δ Temperature	
Location	% Urban[a]	Δ Albedo	Summer (JJA)	Winter (DJF)
Columbus, OH	20%	0.02	−0.02[b]	−0.05
San Antonio, TX	27%	0.03	−0.08[b]	−0.10
San Diego, CA	28%	0.03	−0.13	−0.11
Jacksonville, FL	28%	0.03	+0.01[b]	−0.06
San Jose, CA	29%	0.03	−0.23	−0.10
Dallas, TX	42%	0.05	−0.09[b]	−0.08[b]
Phoenix, AZ	47%	0.05	−0.16	−0.19
Miami, FL	54%	0.06	−0.11	−0.12
Chicago, IL	61%	0.07	−0.27	−0.12
Atlanta, GA	70%	0.08	−0.12	−0.21
Philadelphia, PA	75%	0.09	−0.22	−0.22
Houston, TX	86%	0.10	−0.19	−0.24
New York, NY	91%	0.10	−0.30	−0.24
Detroit, MI	95%	0.11	−0.39	−0.12
Los Angeles, CA	96%	0.11	−0.53	−0.41

[a] Percentage of land area classified as urban.
[b] Indicates the temperature change is not significantly different from 0.

Surface incident shortwave radiation based on satellite measurements of clouds, and the Mosaic land-surface transfer model from the Global Land Data Assimilation System (Rodell *et al* 2004) was compared with simulated values that are a function of latitude, season and cloud cover. The modeled incident shortwave radiation was ∼10% higher across much of the domain (see supplemental figure 3 available at stacks.iop.org/ERL/6/034001/mmedia) compared with the measured data.

In general, model simulations compared well with observations with some biases in precipitation notably. Other work has extensively evaluated the capability of WRF to act as a regional climate model, for example see Zhang *et al* (2009).

3. Results and discussion

3.1. Cool surfaces: urban brightening

A comparison of 2 m temperatures between CTRL and COOL (see figure 2) shows year-round temperature reductions in cities and some rural areas, hatched areas designate changes significantly different from 0. Mean afternoon (1 pm PST) temperature changes due to increased urban albedo ranged from −0.64 °C to +0.27 °C and −0.41 °C to +0.07 °C, in the summer and winter, respectively. Some temperature increases are found during summertime and in regions with low urbanization. Differences between CTRL and COOL arise due to the modeled surface albedo brightening in urban areas and do not reflect changes to air conditioning and waste heat from buildings. Waste heat from buildings is a non-negligible but small portion of the total anthropogenic heat flux in urban areas, and is discussed further by Synnefa *et al* (2008).

Table 1 shows temperature and albedo changes at 15 urban regions including the ten most populated urban areas and five other areas of interest. For the urban areas in table 1, the magnitude of the albedo change can account for ∼60% of the

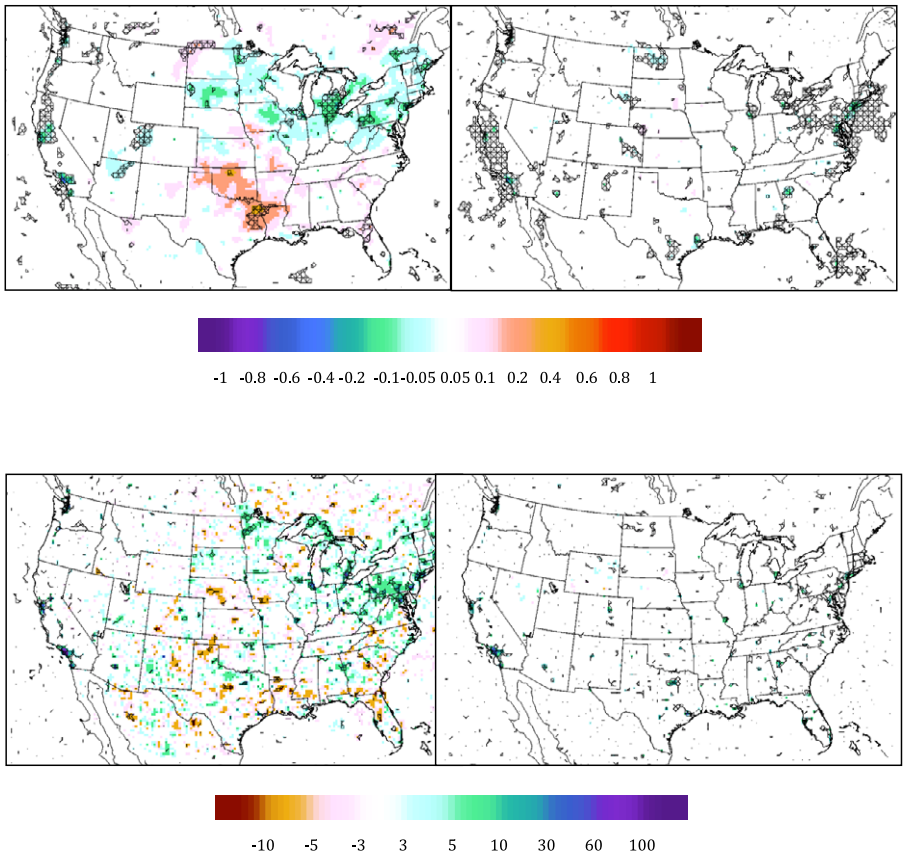

Figure 2. 12-year average difference (COOL–CTRL) at 1 pm PST (2100 UTC). Top: 2 m air temperature (°C) Bottom: top of atmosphere outgoing shortwave radiation (W m^{-2}). Hatched areas show 95% confidence level that diagnostic is different from zero. Left: summer (JJA). Right: winter (DJF).

variance in the temperature change in both seasons. Some urban areas are more sensitive to albedo changes than others. For example, San Diego, CA, and Jacksonville, FL were modeled with an increase in urban albedo of 0.03, however, in San Diego, the average summer afternoon temperatures decreased by 0.13 °C whereas Jacksonville saw no significant change from the base scenario temperatures. In fact, the region directly southeast of Jacksonville showed significant increases in summer afternoon temperatures under the COOL scenario. During the winter period, both San Diego and Jacksonville showed a similar response to albedo changes (∼–0.1 °C).

Regions with elevated temperatures in COOL are associated with lower soil moisture, fewer or thinner clouds, and less precipitation (see supplemental figure 4 available at stacks.iop.org/ERL/6/034001/mmedia). In Texas and the southeast, reduced precipitation is due to reduced cumulus precipitation. For the regions with increased temperatures located in the north, precipitation reductions were due to changes in both cumulus and grid-scale precipitation. An additional feedback effect is seen in non-urban regions in the northeastern portion of the domain where reduced temperatures in COOL are associated with increased cloudiness. Albedo changes in COOL cause feedback effects that both amplify and mitigate local urban cooling. The feedback effects seen in this experiment are the product of both local and domain-wide changes, thus we cannot explain temperature increases as the direct result of a local surface change.

Similar to this work, Menon *et al* (2010), modeled adoption of cool roofs and pavements across the US, however they did not include coupling of the land-surface model to atmospheric circulation scheme. Comparison of our results to Menon *et al* (2010) illustrate the impact of atmospheric feedback on temperature and radiative effects from urban albedo changes. Table 2 shows summertime differences in temperature and outgoing radiation between COOL and CTRL as well as corresponding values reported by Menon *et al* (2010). As expected the fully coupled model shows greater regional variability, with differences in temperature normalized to albedo change ranging from −23 °C in California to +42 °C in Texas, compared to Menon *et al* (2010), where normalized temperature differences ranged from −3 to −6 °C across all regions. Additionally, radiation changes reported in table 2 showed high seasonal and annual variability. During the summertime, over the full national domain, and normalized to albedo change, we found summer temperature and summer total outgoing radiation changes of −5 °C and +282 W m^{-2}, compared to −3 °C and +182 W m^{-2} found by Menon *et al* (2010). Thus, despite some regional warming influences, the increase in urban albedo lead to increased outgoing radiation over the full domain.

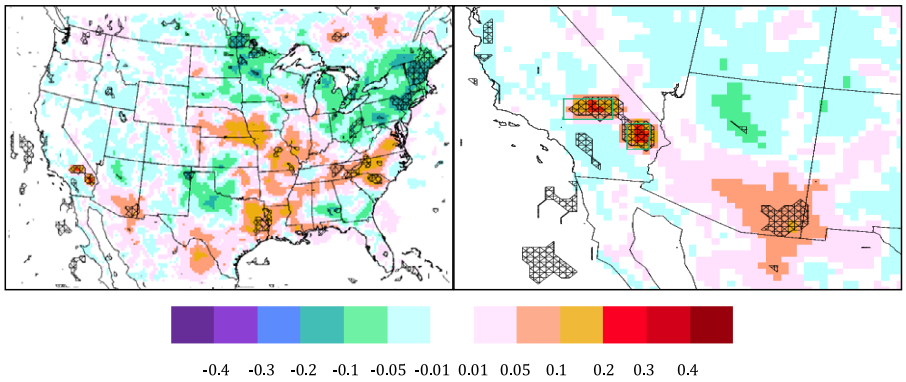

Figure 3. 12-year average difference (SOL–CTRL) at 1 pm PST (2100 UTC). 2 m air temperature (K). Hatched areas show 95% confidence level that diagnostic is different from zero. Left: full domain. Right: expanded detail near solar arrays (arrays outlined in green).

Table 2. Summer (annual) all-hour average values for COOL minus CTRL over specified domains. (N. California: 36.25°–42.25°N and 115.25°–124.25°W. Florida: 24.25°–31.25°N and 79.25°–87.15°W. Texas: 25.25°–36.75°N and 93.25°–106.75°W. US: 25.25°–48.75°N and 67.75°–124.75°W.) (Note: for comparison, shaded areas show summer values from Menon *et al* (2010) tables 2–5.)

	Albedo	Surface temperature (°C)	Total outgoing radiation (W m^{-2})	Outgoing longwave radiation (W m^{-2})	Outgoing shortwave radiation (W m^{-2})
N. California	0.000 49	−0.011 (−0.009)	0.12 (0.10)	−0.02[a] (−0.02)[a]	0.14 (0.11)
Florida	0.002 00	0.009[a] (−0.002)[a]	0.22[a] (0.27)	0.05[a] (0.03)[a]	0.16[a] (0.24)
Texas	0.000 59	0.025[a] (0.010)[a]	−0.06[a] (0.08)	0.03[a] (0.01)[a]	−0.09[a] (0.07)[a]
US	0.000 86	−0.004[a] (−0.005)[a]	0.24 (0.16)	−0.01[a] (−0.01)[a]	0.26 (0.17)
N. California	(normalized	−23 (−17)	250 (194)	−42 (−35)	290 (229)
Florida	to Δ albedo)[b]	4 (−1)	110 (138)	25 (17)	83 (121)
Texas		42 (17)	−97 (130)	54 (9)	−148 (121)
US		−5 (−6)	282 (184)	−17 (−12)	299 (196)
N. California	(normalized	−6	200	−30	230
Florida	to Δ albedo)[b]	−3	175	−17	192
Texas		−5	170	−30	200
US		−3	182	−18	200

[a] Indicates temperature or radiation change is not significantly different from 0.

[b] Surface temperature, shortwave outgoing radiation, longwave outgoing radiation, and total outgoing radiation, have been normalized by the mean land based albedo change of each region.

3.2. Hot surfaces: desert PV

For the 30 grid cells that comprised the simulated desert solar arrays, albedo was reduced by an average of −0.05 (from ∼0.21 to 0.16). The 16% 'effective' albedo for the solar arrays was based on 11% efficiency and 5% reflectance. Temperature in SOL increased by up to +0.4 °C directly over the areas with reduced albedo and smaller but significant temperature effects were seen elsewhere (hatched areas in figure 3) across the domain.

The solar arrays influence local and regional wind patterns and boundary layer height. The changes found are due only to surface albedo changes, surface roughness, for example, was held constant across all scenarios. Although not modeled here, some changes to wind patterns and turbulent flux would be expected if surface roughness parameters were altered. Supplemental figure 5 (available at stacks.iop.org/ERL/6/034001/mmedia) shows a 12-year summer average diurnal cycle of CTRL wind vectors and of the difference in wind vectors between SOL and CTRL. Directly above the solar arrays there is an increase in the magnitude of the afternoon southwesterly winds. Directly downwind of the arrays the magnitude of the prevailing afternoon southwesterly winds is reduced. The temperature and wind differences are also associated with higher afternoon boundary layer heights (150–250 m increase) over the solar arrays. It is interesting to note that supplemental figure 5 (available at stacks.iop.org/ERL/6/034001/mmedia) shows the disturbance in wind patterns caused by the solar arrays shifts downwind after sunset and directly effects nighttime wind patterns over Nevada and Arizona up to 300 km from the solar arrays.

Significant changes to total outgoing radiation are seen locally as well, outgoing shortwave radiation is reduced by 40–75 W m^{-2} directly over the solar arrays, and outgoing longwave radiation increased by 1–5 W m^{-2}. Note that by including the efficiency of the solar panels in the albedo calculation we model energy sent to the transmission grid as reflected back into space. This technique allows us to accurately model the local surface temperature in SOL but causes us to overstate outgoing shortwave radiation directly over the solar arrays by <110 W m^{-2}. However, when considering the domain-wide energy balance, our model is accurate given the assumption that electricity generated by the solar arrays reduces electricity generated from other sources.

Table 3. CO_2 offsets equivalent to increased radiative forcing from urban albedo brightening for US domain (25.25°–48.75°N and 67.75°–124.75°W).

Variable	Summer values	Annual values
Average increase in outgoing radiation (±95% C.I.) (W m^{-2})	0.24 ± 0.07	0.16 ± 0.03
Top of atmosphere radiative change per Δ atmospheric CO_2 (kW t^{-1} CO_2)	0.91	0.91
Grid cells (land only) in US domain	16 003	16 003
Atmospheric CO_2 equivalent (±95% C.I.) for albedo changes under the COOL scenario (Gt CO_2)	2.7 ± 0.8	1.8 ± 0.3
Emitted CO_2 equivalent offset (±95% C.I.) for albedo changes under the COOL scenario (Gt CO_2)	4.9 ± 1.5	3.3 ± 0.5
Offset (±95% C.I.) per cool roof area (kg CO_2 m^{-2})	262 ± 78	175 ± 33
Offset (±95% C.I.) per cool pavement area (kg CO_2 m^{-2})	187 ± 56	125 ± 24

Averaged over all summer hours and the US domain as defined in table 2, we find temperature and total outgoing radiation differences (SOL − CTRL) of -0.001 ± 0.01 °C (mean ± 95% C.I.) and 0.04 ± 0.08 W m^{-2} (mean ± 95% C.I.). These temperature and radiation differences are not significant and we are not able to discern any continental pattern of increased radiative forcing due to the Mojave Desert solar installations. Unlike the SOL simulation, the radiative changes from the COOL simulation were significant as an increase in outgoing radiation was found across the full US domain.

The domain-wide temperature response in SOL is likely dependent on the particular location and parameters of the simulated solar arrays whereas the local response in SOL may be more robust. Evidence that the local temperature response to albedo changes is robust in the Southwest can be found from the COOL results: San Jose, Los Angeles, San Diego and Phoenix show a similar local temperature response to urban brightening when normalized by the albedo change with an average and standard deviation of -4.6 ± 1.6 °C for summer 1 pm PST. In SOL, the average and standard deviation of normalized 1 pm PST temperature change for the 30 grid cells that comprise the solar arrays is -3.1 ± 1.6 °C.

3.3. CO_2 offsets from radiative forcing

Differences in outgoing radiation and albedo between COOL and CTRL over the US domain (see table 2) are used to calculate the radiative forcing obtained for the changes in albedo. Results here can be compared to Menon *et al* (2010) by normalizing the radiative forcing changes to the albedo changes. The summer RF01A (Δ radiative forcing normalized to a 0.01 change in albedo) of 2.8 W m^{-2} is ∼55% greater than the RF01A found using an uncoupled land-surface model (Menon *et al* 2010), and reflects differences between the setup of the two models and that atmospheric feedbacks from urban albedo changes not only attenuate forcing changes but amplify the changes in some regions.

The RF01A averaged over the full annual cycle is 1.8 W m^{-2}. The annual RF01A is similar (within 15%) to boreal summer estimates in Menon *et al* (2010), however the past work did not include full annual cycles for comparison. Equivalent CO_2 offsets (see table 3) were based on the assumptions used by Menon *et al* (2010) and Akbari *et al* (2009) that top of atmosphere radiative change is 0.91 kW per increased ton of atmospheric CO_2 and that 55% of emitted CO_2 is retained in the atmosphere. Our domain classified an area of 7.5×10^{10} m^2 as urban, and assuming 25% and 35% of urban area is roof and pavement, respectively, we find that brightening all urban surfaces in the US could offset 3.3 ± 0.5 Gt of CO_2 emissions or 175 ± 33 kg CO_2 m^{-2} modeled roof area and 125 ± 24 kg CO_2 m^{-2} modeled pavement area (mean ± 95% C.I.). We base this offset on the annual values of radiative forcing as opposed to the higher summer radiative forcing. As past work has focused only on summer changes to radiative forcing, it is of interest to note the annual change to radiative forcing is ∼33% lower compared to summer changes to radiative forcing.

The statistical confidence presented above and in tables 1–3 and figures 2 and 3 reflects only interannual variability in the modeling results. Other uncertainties are not reflected, such as the uncertainties in the top of the atmosphere forcing from atmospheric CO_2 and in the percentage of emitted CO_2 that is retained in the atmosphere, as discussed by Menon *et al* (2010) and Akbari *et al* (2009). Additionally, the total urban area in the domain is uncertain and changes over time. The urban area defined in our domain was relatively low (∼0.7%) compared to other urban land estimations such as those based on MODIS satellite data with >1% of the land area classified as urban. Given the non-linearity of the system it is not clear that increasing urban land area would lead to a one-to-one increase in potential CO_2 emission offsets from cool roof and pavement adoption. An additional uncertainty is how urban smog, precursor emissions, and atmospheric chemistry interact with changes due to surface brightening. Urban smog was not modeled here, and future work is needed to determine the interaction between surface brightening and local and regional pollutants. It should also be noted that within building energy savings due to cool roofs are not included in the estimate of CO_2 offsets.

3.4. Impact of low albedo desert PV

The conversion of the 30 grid cells to solar arrays has the potential to generate up to one terawatt of power given the assumptions of 11% efficiency and that panels cover roughly half the area in each grid cell. A terawatt of peak solar power capacity may offset a gigaton of CO_2 emissions per year (Kantner *et al* 2009) which corresponds to an offset of 107 kg CO_2 m^{-2} $year^{-1}$ of solar panels modeled here. The domain-wide differences in outgoing radiation between SOL

and CTRL were not significantly different from zero, thus a corresponding carbon penalty due to the low albedo of the PV arrays cannot be estimated. An issue here is the choice of domain over which to analyze the effects of solar installation. A small domain centered on the Mojave Desert may indicate a significant decrease in outgoing radiation, a result not found when the full continent is included in the analysis. It is thus important to include a large domain and a coupled land–atmosphere system to investigate the effects of installations of large-scale solar arrays.

Although we investigated the effects of decreasing the surface albedo with PV, it is important to note that despite its dark appearance solar generation can have a local cooling effect in situations where the efficiency of the panel is larger than the background albedo. For example, a majority of the land area in CTRL was classified with a background albedo $<18\%$ but some commercial PV panels currently reach $>18\%$ efficiency and concentrating PV technology can reach higher efficiencies. Nemet (2009) assumes the efficiency of PV panels will reach 28% by 2100. With efficiencies of 28% PV panels will provide local cooling effects in most regions.

4. Conclusions

Here we have examined the regional climate effects of cool roof and cool pavement adoption. At the grid cells containing the 10 most populous cities we found average ($\pm$ standard deviation) afternoon temperature reductions of $0.22 \pm 0.13\,^{\circ}\mathrm{C}$ and $0.18 \pm 0.02\,^{\circ}\mathrm{C}$ in the summer and winter, respectively, under the cool surface scenario. No large urban areas showed significant increases in afternoon temperatures under the cool surface scenario.

We found our coupled land-surface atmospheric model allowed us to identify atmospheric feedbacks that, depending on the region, amplified or reduced temperature and radiative forcing effects due to increased urban albedo during the summertime. Including these feedbacks we showed larger normalized reductions for temperature and radiative forcing under our cool surface scenario compared to past studies.

The equivalent one-time carbon offsets due to brightening urban surfaces was 3.3 ± 0.5 Gt of CO_2, corresponding to 175 ± 33 kg CO_2 m^{-2} of roof area and 125 ± 24 kg CO_2 m^{-2} of pavement area (mean $\pm$ 95% C.I.). We found the large-scale adoption of desert PV lead to significant local temperature increases ($+0.4\,^{\circ}\mathrm{C}$) and regional changes in wind patterns. Unlike the cool surfaces scenario, the solar array scenario showed no significant change to domain-wide outgoing radiation. In the solar array scenario, the relatively high interannual variability of changes to domain-wide outgoing radiation obscured more consistent local and regional effects of the solar arrays.

Ongoing work on these topics aims to incorporate atmospheric chemistry and treatment of potential changes to emissions from electric power generation due to adoption of both cool roof and PV technologies. Additional studies may also test the sensitivity of these results to various model parameters and land-use assumptions including deployment of solar arrays.

Acknowledgments

The work at Lawrence Berkeley National Laboratory was supported by the US Department of Energy under Contract No. DE-AC02-05CH1123. The Laboratory Directed Research and Development Program at LBNL and the DOE Atmospheric System Research Program supported this research. We would like to acknowledge Paul Alivisatos, Director of LBNL, for providing the motivation for the PV research, and Art Rosenfeld for helping to motivate the cool roof research. This research used resources from LBNL's Lawrencium and the DOE's National Energy Research Scientific Computing Center.

References

Acker J G and Leptoukh G 2007 Online analysis enhances use of NASA earth science data *EOS Trans. AGU* **88** 14

Akbari H 2003 Measured energy savings from the application of reflective roofs in two small non-residential buildings *Energy* **28** 953–67

Akbari H, Bretz S, Kurn D M and Hanford J 1997 Peak power and cooling energy savings of high-albedo roofs *Energy Build.* **25** 117–26

Akbari H and Konopacki S 2005 Calculating energy-saving potentials of heat-island reduction strategies *Energy Policy* **33** 721–56

Akbari H and Levinson R 2008 *Status of Cool Roof Standards in the United States* (Berkeley, CA: Lawrence Berkeley National Laboratory) (available at http://escholarship.org/uc/item/5cg147dp)

Akbari H, Menon S and Rosenfeld A 2009 Global cooling: increasing world-wide urban albedos to offset CO_2 *Clim. Change* **94** 275–86

Campra P, Garcia M, Canton Y and Palacios-Orueta A 2008 Surface temperature cooling trends and negative radiative forcing due to land use change toward greenhouse farming in southeastern Spain *J. Geophys. Res.* **113** D18109

CEC 2010a *Abengoa Mojave Solar Project, Commission Decision* CEC-800-2010-008 CMF, Docket Number 09-AFC-5 (Sacramento, CA: California Energy Commision) (available at http://www.energy.ca.gov/sitingcases/abengoa/index.html)

CEC 2010b *Genesis Solar Energy Project, Commission Decision* CEC-800-2010-011 CMF, Docket Number 09-AFC-8 (Sacramento, CA: California Energy Commision) (available at http://www.energy.ca.gov/sitingcases/genesis_solar/index.html)

Chen F and Dudhia J 2001 Coupling an advanced land surface-hydrology model with the penn state-NCAR MM5 modeling system. Part I: model implementation and sensitivity *Mon. Weather Rev.* **129** 569–85

Csiszar I and Gutman G 1999 Mapping global land surface albedo from NOAA AVHRR *J. Geophys. Res.* **104** 6215–28

Ek M B *et al* 2003 Implementation of Noah land surface model advances in the national centers for environmental prediction operational mesoscale eta model *J. Geophys. Res.* **108** 8851

GISS 2010 *GISS Surface Temperature Analysis, Station Data* (New York: Goddard Institute for Space Studies) (available at http://data.giss.nasa.gov/gistemp/station_data)

Kantner J, Mileva A and Kammen D 2009 *Gigaton Throwdown, Chapter: Solar Photovoltaics* (San Francisco, CA: Gigaton Throwdown Initiative) (available at http://www.gigatonthrowdown.org)

Lin Y L, Farley R D and Orville H D 1983 Bulk parameterization of the snow field in a cloud model *J. Clim. Appl. Meteorol.* **22** 1065–92

Lynn B H *et al* 2009 A modification to the NOAH LSM to simulate heat mitigation strategies in the New York City metropolitan area *J. Appl. Meteorol. Climatol.* **48** 199–216

Menon S *et al* 2010 Radiative forcing and temperature response to changes in urban albedos and associated CO_2 offsets *Environ. Res. Lett.* **5** 014005

Mesinger F *et al* 2006 North American regional reanalysis *Bull. Am. Meteorol. Soc.* **87** 343–60

Nemet G F 2009 Net radiative forcing from widespread deployment of photovoltaics *Environ. Sci. Technol.* **43** 2173–8

NOAA 2004 *Climatography of the United States NO. 20, Monthly Station Climate Summaries, 1971-2000* (Asheville, NC: National Oceanic and Atmospheric Administration) (available at http://www.ncdc.noaa.gov/oa/climate/normals/usnormals.html)

NWS 2010 *Advanced Hydrologic Prediction Service* (MD: National Weather Service) (available at http://water.weather.gov/)

Oleson K W, Bonan G B and Feddema J 2010 Effects of white roofs on urban temperature in a global climate model *Geophys. Res. Lett.* **37** L03701

Pomerantz M *et al* 1999 Reflective surfaces for cooler buildings and cities *Phil. Mag.* B **79** 1457–76

Reynolds R W *et al* 2007 Daily high-resolution-blended analyses for sea surface temperature *J. Clim.* **20** 5473–96

Rodell M *et al* 2004 The global land data assimilation system *Bull. Am. Meteorol. Soc.* **85** 381–94

Skamarock W C *et al* 2008 A description of the advanced research WRF version 3 *NCAR Technical Note NCAR/TN-475+STR* (Boulder, CO: National Center for Atmospheric Research) (available at www.mmm.ucar.edu/wrf/users/pub-doc.html)

Synnefa A, Santamouris M and Kolokotsa D 2009 Promotion of cool roofs in the EU—The Cool Roofs Project *Second Int. Conf. on Countermeasures to Urban Heat Islands (Berkeley, CA)* (available at http://heatisland2009.lbl.gov/docs/231120-synnefa-doc.pdf)

Synnefa A *et al* 2008 On the use of cool materials as a heat island mitigation strategy *J. Appl. Meteorol. Climatol.* **47** 2846–56

Taha H 2008a Episodic performance and sensitivity of the urbanized MM5 (uMM5) to perturbations in surface properties in Houston Texas *Bound. Layer Meteorol.* **127** 193–218

Taha H 2008b Meso-urban meteorological and photochemical modeling of heat island mitigation *Atmos. Environ.* **42** 8795–809

Taha H 2008c Urban surface modification as a potential ozone air-quality improvement strategy in California: a mesoscale modelling study *Bound. Layer Meteorol.* **127** 219–39

Zhang Y X, Dulière V, Mote P W and Salathé E P Jr 2009 Evaluation of WRF and HadRM mesoscale climate simulations over the US Pacific Northwest *J. Clim.* **22** 5511–26

Zhou Y and Shepherd J M 2009 Atlanta's urban heat island under extreme heat conditions and potential mitigation strategies *Nat. Hazards* **52** 639–68